Biotechnol Lett (2023) 45:551–561
https://doi.org/10.1007/s10529-023-03361-3

ORIGINAL RESEARCH PAPER

Inactivation of SARS-CoV-2 variants by nitrogen-doped titanium dioxide loaded with metals as visible-light photocatalysts

Takashi Matsuyama · Shu Saeki · Satoru Kosaka · Yoriko Matsuoka · Yoshifumi Aoki · Yasushi Itoh · Takao Imaeda

Received: 6 July 2022 / Revised: 18 November 2022 / Accepted: 10 February 2023 / Published online: 13 March 2023

Abstract

Purpose We examined the inactivation of severe acute respiratory syndrome coronavirus 2 (SARS-CoV-2) by a nitrogen-doped titanium dioxide (N-TiO_2) visible-light photocatalyst that was activated via light irradiation in the natural environment and was safe for human use as a coating material.

Methods The photocatalytic activity of glass slides coated with three types of N-TiO_2 without metal or loaded with copper or silver and copper was investigated by measuring acetaldehyde degradation. The titer levels of infectious SARS-CoV-2 were measured using cell culture after exposing photocatalytically active coated glass slides to visible light for up to 60 min.

Results N-TiO_2 photoirradiation inactivated the SARS-CoV-2 Wuhan strain and this effect was enhanced by copper loading and further by the addition of silver. Hence, visible-light irradiation using silver and copper-loaded N-TiO_2 inactivated the Delta, Omicron, and Wuhan strains.

Conclusion N-TiO_2 could be used to inactivate SARS-CoV-2 variants, including emerging variants, in the environment.

Keywords Nitrogen-doped titanium dioxide · SARS-CoV-2 · Viral inactivation · Visible-light photocatalyst

Supplementary Information The online version contains supplementary material available at https://doi.org/10.1007/s10529-023-03361-3.

T. Matsuyama (✉) · S. Saeki · S. Kosaka · Y. Matsuoka · Y. Aoki · T. Imaeda
Toyota Central Research and Development Laboratories Incorporated, Nagakute 480-1192, Japan
e-mail: e1215@mosk.tytlabs.co.jp

S. Saeki
e-mail: e1347@mosk.tytlabs.co.jp

S. Kosaka
e-mail: e1077@mosk.tytlabs.co.jp

Y. Matsuoka
e-mail: yoriko@mosk.tytlabs.co.jp

Y. Aoki
e-mail: e1098@mosk.tytlabs.co.jp

T. Imaeda
e-mail: e0914@mosk.tytlabs.co.jp

Y. Itoh
Shiga University of Medical Science, Otsu 520-2192, Japan
e-mail: yasushii@belle.shiga-med.ac.jp

Introduction

Over the recent years, the severe acute respiratory syndrome coronavirus 2 (SARS-CoV-2) pandemic has caused significant health and economic losses worldwide (Zhou et al. 2020). Constant inactivation of the virus in the environment is crucial to prevent the spread of SARS-CoV-2, which is transmitted

mainly through aerosols emitted by infected persons (Prather et al. 2020). Infectious viruses have also been detected on the surfaces of objects in public places, such as hospitals (Feng et al. 2021), which are widely disinfected using alcohol or other agents (Kampf et al. 2005). However, the coating of various surfaces using solid antiviral compounds was shown to provide sustained antiviral effectiveness (van Doremalen et al. 2020). For antimicrobial coatings, the use of various compounds that can kill or inhibit the growth of pathogens, fungi, and viruses has been considered (Rai et al. 2020). Among these compounds, visible-light photocatalysts are promising as they can degrade organic molecules via oxidative chemicals generated by light irradiation from indoor lighting fixtures (Matsuura et al. 2021; Uema et al. 2021; Nakano et al. 2022; Prakash et al. 2022). The effectiveness of visible-light photocatalysts, titanium dioxide (TiO_2) loaded without metal (Matsuura et al. 2021), tungsten trioxide (WO_3) with unknown additives (Uema et al. 2021), and TiO_2 loaded with nanoclusters of copper oxide (Nakano et al. 2022) for the inactivation of SARS-CoV-2 has been previously reported. However, the effect of additive metals on viral inactivation by main component oxides remains to be elucidated. The inactivation of SARS-CoV-2 using silver (Ag) nanoparticles has been proposed (Pilaquinga et al. 2021), although the effects of Ag as an additive for visible-light photocatalysts remain unclear. The present study revealed that the efficacy of SARS-CoV-2 inactivation was enhanced by loading Ag or copper (Cu) on nitrogen-doped titanium dioxide (N-TiO_2), which is a visible-light photocatalyst (Asahi et al. 2001, 2014; Morikawa et al. 2006; Ohwaki et al. 2016). We also showed that N-TiO_2 loaded with both Ag and Cu could inactivate the SARS-CoV-2 Delta and Omicron variants that temporarily dominated the pandemic.

Materials and Methods

N-TiO_2 coating of glass surfaces

We evaluated three types of visible photocatalysts: N-TiO_2 (Toyotsu Vehitecs Co., Ltd., VCT-01SQC), Cu-loaded Cu/N-TiO_2 (Toyotsu Vehitecs Co., Ltd., VCTIIC-01SQC), and Cu + Ag/N-TiO_2 (N-TiO_2 loaded with both Cu and Ag; Toyotsu Vehitecs Co., Ltd., VCTIICA-01). These photocatalysts were synthesized based on the flowchart depicted in Fig. 1. N-TiO_2 powder with 0.25% nitrogen doping for oxygen was obtained by annealing the anatase-type TiO_2 powder with the nitrogen source (Asahi et al. 2001; Morikawa et al. 2006). The crystal structure of the powder was evaluated using X-ray diffraction (XRD) (SU3500, Rigaku, Japan) analysis, and the optical absorption edge was measured via ultraviolet–visible absorption spectroscopy (V-780, JASCO, Japan). Cu or Cu and Ag loading were prepared by impregnating N-TiO_2 with an aqueous solution of $Cu(NO_3)_2$ or $AgNO_3$ at room temperature, followed by stirring, washing, and filtration. Each powder was finely ground, water-slurried, and mixed with an organic binder to prepare the photocatalytic coating solutions with 6% solid content. The size distribution of the dispersed particles in the coating solution was evaluated using dynamic light scattering analysis (DLS) (Zetasizer Nano ZSP, Malvern Panaltical). Glass slides or 5-cm square glass plates (Matsunami Glass Ind., Ltd., S1111) were sonicated in acetone and ethanol for 10 min each and then dried at 80 °C for 1 h. Coating solution (0.8 mL) was dropped onto the washed glass and spin-coated at 750 rpm for 5 s. The samples were then heat-treated at 200 °C for 1 h

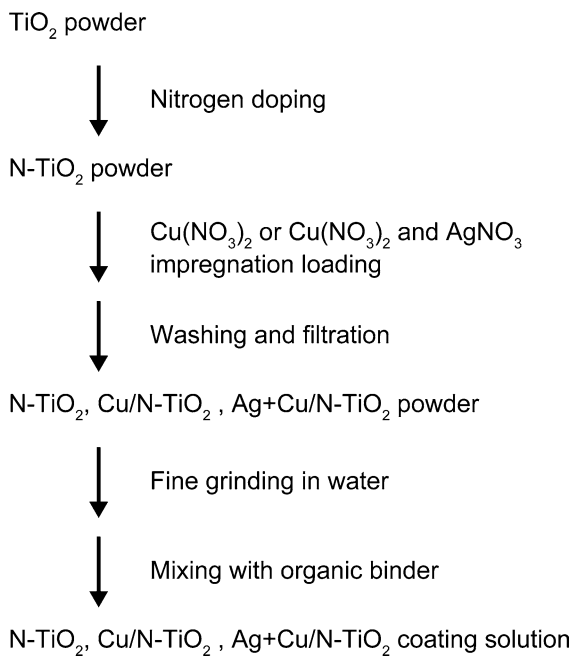

Fig. 1 Flowchart of the synthesis process of photocatalyst coating solution

and ultraviolet-irradiated using a black light for 1 h to remove surface deposits before use in the subsequent experiments.

Qualitative analysis on reactive oxygen radicals

Reactive oxygen species generated by photocatalysts was qualitatively analyzed using the spin-trap ESR (Electron Spin Resonance) method. 5,5-dimethyl-1-pyrroline N-oxide (DMPO) (Tokyo Chemical Industry Co., Ltd.) was used as the spin-trapping reagent. DMPO was diluted with water to 5 mol/dm^3, purified using spherical activated carbon (AS ONE CORPORATION), and finally used as a spin-trap solution. After spreading 100 µL of the solution on each N-TiO_2-coated glass plate at a depth of ~ 4 cm^2 and irradiated with visible light at 10,000 lx for 15 min, ~ 75 µL of the reaction solution was collected and measured using X-band ESR (Bruker E500). The measurement conditions were microwave power, 3.17 mW; microwave frequency, 9.82 GHz; modulation amplitude, 0.2 mT; modulation frequency, 100 kHz; time constant, 30 ms; receiver gain, 60; magnetic field scan, 20 mT; and scan, 10.

Observation using scanning electron microscopy and quantification by inductively coupled plasma

The surface condition of the glass coated with N-TiO_2 was examined via scanning electron microscopy (SEM) (Hitachi High-Tech Co., Regulus 8230). The coated glass slides were cut into 10-mm squares, further coated with osmium, and secondary electron images were captured at an acceleration voltage of 2 keV. Acid dissolution of N-TiO_2 coated on the glass surface was performed and the Ti content of each sample was quantified via inductively coupled plasma optical emission spectroscopy (ICP–OES) (Hitachi High-Tech Science Co., PS3520UVDDII). The Cu and Ag contents were quantified using ICP mass spectrometry (ICP–MS) (Agilent Technologies, Agilent 8900). The TiO_2 content was estimated by calculating the Ti content, and the total $TiO_2 + Cu + Ag$ content was used as the sample total weight.

Photocatalytic activity evaluation

The photocatalytic activity of N-TiO_2 was evaluated using an acetaldehyde degradation test. The 5-cm square glass plates coated with each type of N-TiO_2 were placed in 500-mL glass containers, filled with air composition levels of O_2/N_2 gas and 60 ppm acetaldehyde gas, sealed, and left in the dark for 1 h, which was considered 0 h. The concentration of acetaldehyde and its degradation product, CO_2, were measured via gas chromatography (Shimadzu Co., GC-14B) under conditions of visible-light irradiation. The fluorescent light of illuminance at 10,000 lx (T-10A, KONICA MINOLTA, INC.) and light power of 550 µW/cm^2 (UVR-2 UD40 detector, TOPCON CO.) with cut film to omit ultraviolet light at < 400 nm was used as a visible-light source. No changes were observed in light intensity during the pre- and post-experiments. The rate of CO_2 production was calculated via linear regression after subtracting background due to uncoated glass.

Enzyme-linked immunosorbent assay analysis of binding affinity between S-protein and ACE2

Binding affinity assay between S-protein and ACE2 was performed using a partially modified protocol of the COVID-19 Spike-ACE2 binding assay kit II (RayBiotech, Inc.). Briefly, 100 µL of a solution of Fc-tagged SARS-CoV-2 spike receptor binding domain protein (S-protein) diluted with the attached buffer (1× Assay Diluent) was placed on a photocatalyst-coated glass slide under a fluorescent lamp covered with a 400 nm cut filter and irradiated with 10,000 lx light for 0, 15, or 60 min at ~25 °C. The glass slide was placed in a plastic petri dish and covered to prevent drying. The light-irradiated glass slide was transferred to a 50 mL centrifuge tube and centrifuged at 1000 rpm for 30 s to collect the solution. Then, the slide was washed with 100 µL assay solution, which was collected by centrifugation at 1000 rpm for 30 s. The collected reaction solution was placed into 96-well plates whose bottoms were coated with recombinantly expressed ACE2, and enzyme-linked immunosorbent assay was performed. The absorbance was measured at 450 nm at 0, 15, and 60 min (designated A0, A15, and A60, respectively). The percentage of denatured S-protein undetectable by the antibody at 15 and 60 min was calculated as (A0 − A15)/A0 and (A0 − A60)/A0, respectively. Four samples were measured per experiment and all experiments were repeated twice. The results were reported as mean and standard deviation.

Inactivation of SARS-CoV-2 and variants using N-TiO_2 plates

SARS-CoV-2 JP/TY/WK-521/2020 (WK-521; Wuhan strain, GenBank Sequence Accession: LC522975), SARS-CoV-2 hCoV/Japan/TY11-927-P1/2021 (TY11-927; Delta variant, GISAID variant name: EPI_ISL_2158617), and SARS-CoV-2 hCoV-19/Japan/TY38-873/2021 (TY38-873; Omicron variant, GISAID variant name: EPI_ISL_7418017) were kindly provided by Drs. Masayuki Saijo, Mutsuyo Takayama-Ito, Masaaki Sato, and Ken Maeda of the National Institute of Infectious Disease (Tokyo Japan). The viruses were propagated once at the Shiga University of Medical Science in VeroE6/TMPRSS2 cells (JCRB Cell Bank, Osaka, Japan). VeroE6/TMPRSS2 cells were cultured in Dulbecco's Modified Eagle Medium (DMEM; Nacalai Tesque, Kyoto, Japan) supplemented with 10% fetal bovine serum (FBS) and 50 µg/mL each of penicillin, streptomycin, and G418 in 96-well plates for 3 days. The viral solution (500 µL) was placed on 25-cm^2 glass plates coated with N-TiO_2 and then exposed to visible-light for the indicated times. The experiment was conducted in a draft chamber with constant negative pressure from exhaust air to ensure safety, and the temperature of the samples was maintained at ~25 °C. A dilution series of the recovered viral solution was prepared and inoculated onto confluent VeroE6/TMPRSS2 cells that had been washed twice with 100 µL of Hanks' Balanced Salt Solution (HBSS) (Nacalai Tesque). The final concentrations of the viral solutions were ~10^4 to 10^2 $TCID_{50}$/mL, and which were higher than the concentration (10^1 $TCID_{50}$/mL) that confirmed human infection (Killingley et al. 2022). The cells were incubated for 1 h at 37 °C, the solution was then removed via aspiration, and the wells were washed once with 100 µL HBSS media. The wash solution was removed via aspiration, 100 µL DMEM supplemented with 0.1% bovine serum albumin (BSA) was added, and the cells were cultured in an incubator at 37 °C for 3 days. Cytopathic effects were observed under a microscope, and the mean tissue culture infectious dose ($TCID_{50}$) was determined. All viral experiments were performed in the Biosafety Level 3 facility of the Research Center for Animal Life Science, Shiga University of Medical Science. Four samples were measured per experiment and all experiments were repeated twice. The results were calculated as mean and standard deviation.

Results

Synthesis of N-TiO_2 particles

Three types of N-TiO_2 were synthesized using titanium dioxide powder as a raw material to prepare the coatings (Fig. 1). The synthesized N-TiO_2 was in the anatase phase with an average crystallite size of 20 nm (Supplementary Fig. 1) and exhibited optical absorption in the visible-light region of 400–520 nm (Supplementary Fig. 2). Dynamic light scattering analysis of the particle size revealed that all the particles exhibited a similar distribution, with a peak at ~ 28 nm (Fig. 2). These particles were used in further experiments.

Reactive oxygen species produced by the light irradiation of N-TiO_2

The free radical species produced by water molecules via the photocatalytic reaction of N-TiO_2 were analyzed using spin-trap ESR (Figure 3). The three ESR spectra of N-TiO_2 showed the same pattern comprising four signals with amplitude ratios of 1:2:2:1, which were determined to be derived from the adduct of the OH radicals that reacted with the spin-trapping agent DMPO, whereas the other spectral patterns, such as signals derived from superoxide anion and alkyl radicals (Finkelstein et al. 1982;

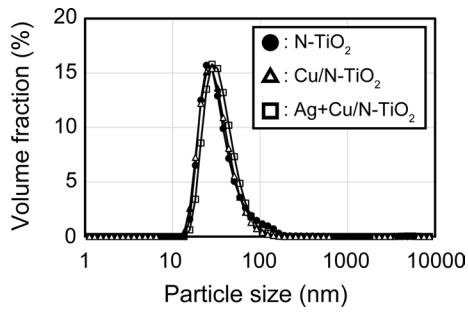

Fig. 2 Particle size distribution of three types of N-TiO_2 used in coating. The vertical axis shows the volume fraction of dispersed particles as measured by dynamic light scattering (DLS)

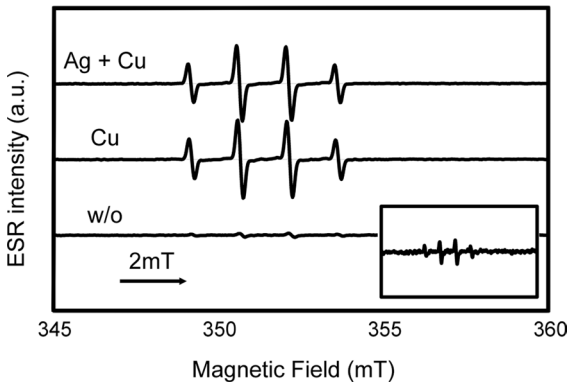

Fig. 3 The ESR spectra of spin traps obtained by visible-light irradiation of N-TiO_2-coated glass plates

Makino et al. 1982), were not detected (Figure 3). Under this light irradiation condition, the chief reactive oxygen species in the reaction solution was found to be OH radicals. The signal intensity of the reaction solution of N-TiO_2 without metal support was < 1/10 of those of the metal-supported N-TiO_2 particles, although not exactly quantitative (Figure 3).

Structure and composition of N-TiO_2 coated on the glass surface

Glass surfaces coated with three types of N-TiO_2 showed agglomerated particles of ~ 20 nm in diameter and pores that were several tens of nm in size (Figure 4). The surface loading of N-TiO_2 and film thickness were ~ 0.5 g/m^2 and ~ 200 nm, respectively, based on the weight increment after coating. The size of the SARS-CoV-2 virus particles ranged from 60 to 140 nm (Zhu et al. 2020); therefore, the viral particles were considered to contact N-TiO_2 at the surface layer without entering the layer when the virus solution was dropped onto the coated glass surface. The compositional analysis of the N-TiO_2 coated on the glass surface using ICP–OES and ICP–MS showed that it contained trace amounts of Cu. Cu/N-TiO_2 contained 3.3 mass% Cu while Ag+Cu/N-TiO_2 contained 1.6 mass% Cu and 0.1 mass% Ag (Table 1).

Visible photocatalytic activity of N-TiO_2

A 5-cm square glass slide coated with each N-TiO_2 was placed in a 500-mL sealed container to measure acetaldehyde degradation activity under visible-light

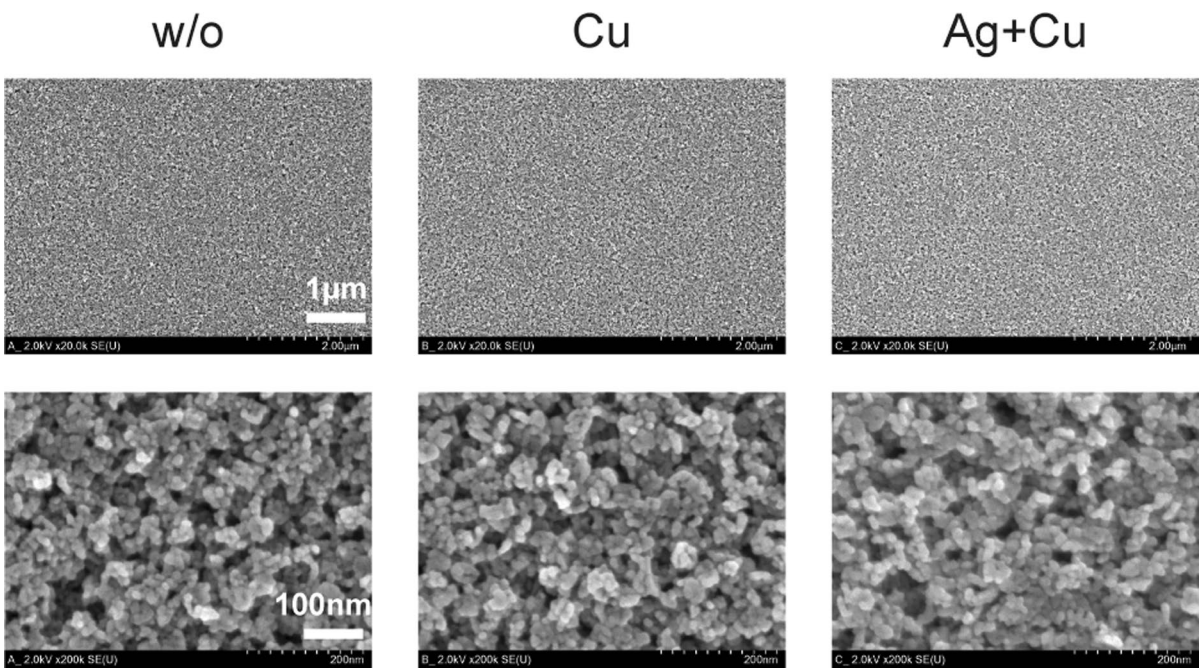

Fig. 4 SEM images of the glass surface coated by three different types of N-TiO_2. w/o, N-TiO_2; Cu, Cu/N-TiO_2; Ag + Cu. Ag + Cu/N-TiO_2

Table 1 Composition of the three types of N-TiO_2 as measured by ICP–MS (mass%)

Sample	Metal/metal oxide		
	TiO_2	Cu	Ag
N-TiO_2	99.9	0.06	< 0.01
Cu/N-TiO_2	96.7	3.3	< 0.01
Ag + Cu/N-TiO_2	98.3	1.6	0.1

Table 2 Rate of carbon dioxide formation following visible-light irradiation of three types of N-TiO_2

Sample	CO_2 formation rate (ppm/h)
N-TiO_2	0.362
Cu/N-TiO_2	0.903
Ag + Cu/N-TiO_2	0.939

irradiation (Fig. 5). For all three types of N-TiO_2, irradiating the coated glass pieces with visible-light decreased the concentration of acetaldehyde in a time-dependent manner, whereas the concentration of the reaction product, CO_2, increased (Fig. 5). The rate of CO_2 formation by metal-loaded N-TiO_2 was ~ 2.5 times faster than that of N-TiO_2 without metal loading. The rates of CO_2 formation were almost equal for Cu/N-TiO_2 (0.903 ppm/h) and Ag + Cu/TiO_2 (0.939 ppm/h) (Table 2).

Inhibition of the binding of S-protein with ACE2 by N-TiO_2

We examined whether the binding of SARS-CoV-2 S-proteins involved in infection with Angiotensin Converting enzyme 2 (ACE2) was inhibited by the photocatalytic activity of N-TiO_2 coated on the glass surface (Fig. 6). When the three types of N-TiO_2 were irradiated with visible-light at 10,000 lx, ~ 70% and > 90% of the S-protein in the solution were not detected by the antibody after 15 and 60 min, respectively, whereas the protein concentration in the reaction solution remained unchanged. After 15- and 60-min light irradiation, there were no significant differences in the proportion of S-protein denaturation between N-TiO_2 without metal loading and Cu/N-TiO_2 ($p = 0.095$ and 0.785) or N-TiO_2 without metal loading and Ag + Cu/N-TiO_2 ($p = 0.068$ and 0.238) that became undetectable with the antibody.

Effects of N-TiO_2 supported by Ag and Cu on SARS-CoV-2 inactivation

The light- and time-dependent inactivation of SARS-CoV-2 (WK-521) by N-TiO_2 with or without metals was investigated using cell culture experiments (Figure 7). To test whether the initial viral titers (7356 $TCID_{50}$/mL) decreased from zero time in N-TiO_2 without metal, it was compared with one of the other samples between the two groups using one-sided *t*-test at a 5% significance level. As a result, no significant difference was detected between the 15- and 60-min dark conditions ($p = 0.074$ and 0.068, respectively); however, a significant difference was detected between the 15 and 60-min light conditions ($p = 0.039$ and 0.010, respectively) (Figure 7 w/o). Based on these results, it was observed that N-TiO_2 without metal could not inactivate SARS-CoV-2 in the dark.

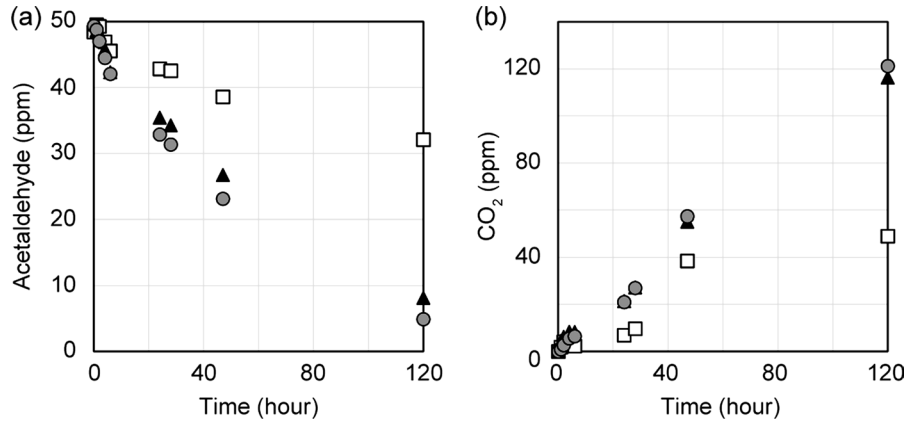

Fig. 5 Acetaldehyde degradation activity of three types of N-TiO_2 under visible-light irradiation. **a** Acetaldehyde degradation. **b** Carbon dioxide formation. White squares indicate N-TiO_2, black triangles indicate Cu/N-TiO_2, and gray circles indicate Ag + Cu/N-TiO_2

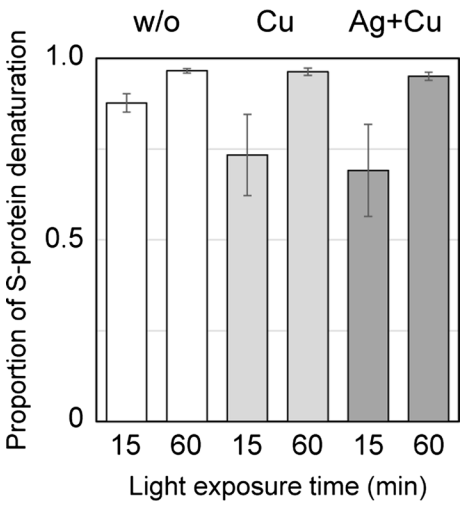

Fig. 6 Denaturation of S-protein by three types of N-TiO_2 irradiated with visible-light. White bars indicate N-TiO_2, light gray bars indicate Cu/N-TiO_2, and dark gray bars indicate Ag + Cu/TiO_2. No significant differences at the 5% level were observed between N-TiO_2 and Cu/N-TiO_2 or Ag + Cu/N-TiO_2 under both the 15- and 60-min light irradiation conditions

Furthermore, under light conditions, some viruses were inactivated after > 15 min of light exposure in this study. Although no significant differences were detected, the mean viral titer at 60 min (2750 $TCID_{50}$/mL) was lower than at 15 min in the light condition (3750 $TCID_{50}$/mL). Significant reductions in the viral titers were observed in the Cu/N-TiO_2 plates under all conditions (Figure 7 Cu). Viral titers decreased by ~ 80% for 15 and 60 min in the dark condition and 15 min in the light condition ($p = 0.013$, 0.013, and 0.016, respectively), and by ~ 3% at 60 min in the light condition ($p = 0.006$). In the light condition, the viral titer at 60 min was significantly reduced to ~ 16% compared with that at 15 min ($p = 0.006$); however, no significant difference was observed in the dark condition ($p = 0.430$). The inactivation of SARS-CoV-2 was also observed on Ag+Cu/N-TiO_2 plates under all conditions (Figure 7 Ag+Cu). In Ag+Cu/N-TiO_2, time-dependent virus inactivation was also detected under dark conditions, with viral titers reaching ~ 24% at 15 min and 4.5% at 60 min compared with that at 0 min ($p = 0.005$ and 0.003, respectively). The light dependence of viral inactivation was also found to be 9.6% at 15 min compared with that at 0 min and < 1% at 60 min under the light conditions ($p = 0.004$ and 0.002, respectively).

Inactivation of SARS-CoV-2 delta and omicron variants

The volume of the infectious viral titers of the SARS-CoV-2 Wuhan, Delta, and Omicron variants were determined using cell culture assay following the visible-light irradiation of Ag+Cu/N-TiO_2-coated glass plates for 60 min. Significant decreases in infectious titers due to light irradiation for 60 min were detected for all three variants compared with the reference

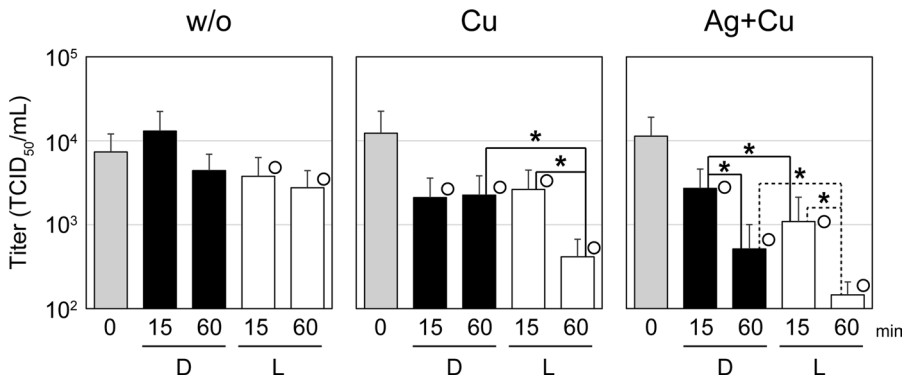

Fig. 7 Inactivation of SARS-CoV-2 (WK-521, Wuhan strain) following visible-light irradiation of three types of N-TiO_2. SARS-CoV-2 virus solution on each N-TiO_2-coated glass was irradiated to visible-light for 0, 15, or 60 min in the dark (D) or light (L). The *y*-axis shows the mean plus standard deviations of the infectious virus titers. Asterisks indicate significant differences of $p < 0.01$ when comparing paired titers, indicated by solid or dotted lines, using one-sided Welch *t*-test. Pairs showing significant differences at $p < 0.05$ when comparing viral titers with one-sided Welch *t*-test are indicated by white circles (at zero time and the sample) and asterisks (pairs indicated by solid or dotted lines)

titers at 0 min (Figure 8). Although a direct comparison among variants could not be conducted owing to the different initial viral concentrations, > 99% of the Wuhan strain, 88.8% of the Delta variant, and 98.6% of the Omicron variant were inactivated following 60 min of light irradiation compared with the viral titers observed at 0 min.

Discussion

The photocatalysis of N-TiO_2 resulted in the degradation of acetaldehyde (Figure 5), conformational changes in S-proteins (Figure 6), and inactivation of SARS-CoV-2 (Figure 7 and Figure 8) in this study. In previous studies, SARS-CoV-2 inactivation by visible photocatalysts TiO_2 (Matsuura et al. 2021) and WO_3 (Uema et al. 2021) was considered to be primarily due to reactive oxygen species generated via light irradiation. Therefore, we hypothesized the following three main reaction fields for N-TiO_2 involved in viral inactivation.

1) Holes on the titanium dioxide surface that oxidizes and decomposes organic matter common to the three types of N-TiO_2.

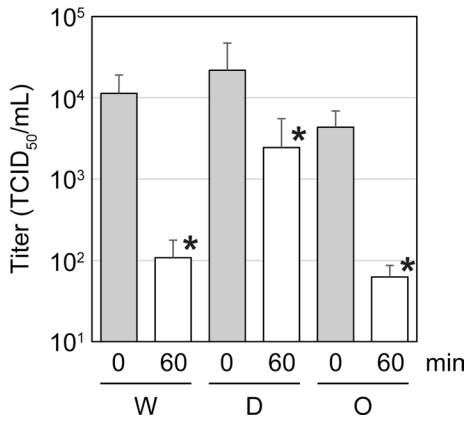

Fig. 8 Inactivation of SARS-CoV-2 variants following visible-light irradiation of Ag + Cu/N-TiO_2. Each bar represents the mean titers of infectious viruses after 0 and 60 min of light irradiation in each variant. The upper side of the standard deviation is indicated. Asterisks indicate significant differences of $p < 0.01$ using a one-sided Welch *t*-test when comparing the tiers after 0 and 60 min of light irradiation in each variant. *W* Wuhan, *D* Delta and *O* Omicron

2) OH radicals produced via water oxidation by the holes.
3) OH radicals generated by the Fenton reaction in the presence of copper through the production of superoxide anions by the combination of excited electrons and oxygen.

We discuss which reaction field was more effective in virus inactivation by N-TiO_2 in the followings.

The photocatalytic degradation of organic compounds, such as acetaldehyde in an aqueous solution, is considered to occur primarily in the hole reaction field created on the photocatalyst surface where these molecules are adsorbed (Zhang and Nosaka 2015), whereas some of them are thought to occur due to OH radicals diffusing into the solution (Asahi et al. 2014). From the results of the acetaldehyde degradation presented in Fig. 5, the holes involved in the oxidative decomposition of organic compounds in N-TiO_2 without metal support were found to be ~ 40% of those in N-TiO_2 with metal support under the same light irradiation conditions. Since electrons excited by visible-light move quickly from N-TiO_2 to Cu in Cu-loaded N-TiO_2 (Kato et al. 2010), we inferred that this difference was attributable to the combination between excited electrons and holes in probability. As no difference was observed in the inhibition of S-protein and ACE protein binding in Fig. 6, the hole reaction field in this experiment was found to be saturated. In the viral inactivation experiment in Fig. 7, the inactivation activity of N-TiO_2 without metal support was observed to be only 1/10 of that of N-TiO_2 with metal support. Based on these results, the mechanisms of action of metal-loaded N-TiO_2 were considered to be direct inactivation via protein adsorption of Cu and Ag and indirect promotion of inactivation. As another mechanism, the inactivation of certain viral biomolecules by oxidation via the OH radicals derived from the Fenton reaction was also considered.

Recently, TiO_2 loaded with copper oxide nanoclusters has been reported to inactivate SARS-CoV-2 even in dark conditions, and light irradiation further enhances this effect (Nakano et al. 2022). This visible photocatalytic virus inactivation was partially caused by Cu(I) species, and the mechanism was considered effective for protein adsorption owing to the solid-phase properties of Cu (Sunada et al. 2012). SARS-CoV-2 inactivation using Ag nanoparticles has also been reported, and the mechanism is considered to be

via protein adsorption as well (Pilaquinga et al. 2021). Adsorption to Cu or Ag could also be considered to attract viral particles near the hole reaction field on the N-TiO_2 surface, resulting in the efficient oxidative degradation of S-proteins or other biochemicals of the virus by the holes.

ESR measurements using the spin-trapping agent DMPO can qualitatively identify multiple reactive oxygen species generated in water (Finkelstein et al. 1980). In the presence of water, the photocatalyst holes react with water molecules to produce free radical species (Kakuma et al. 2015). Using the ESR spectral pattern, only OH radicals were detected in all the samples and no OOH and alkyl radicals, among others, derived from superoxide anions were identified (Figure 3). The amplitude intensity of the ESR spectra derived from OH radicals was stronger in Cu-loaded N-TiO_2 than in N-TiO_2 without metal loading. This difference was not considered to be caused by the hole binding to water, but rather from the Fenton reaction that occurred in the presence of copper. OH radicals are strong oxidants with an oxidation potential of 2.81 eV, which is sufficiently high to inactivate the virus (Koppenol and Liebman 1984; Nakamura et al. 2020). In the viral inactivation experiments shown in Figure 7, both metal-loaded N-TiO_2 inactivated SARS-CoV-2 in a light-irradiated and time-dependent manner. Collectively, these results suggest that the oxidative effect of OH radicals on some viral biomolecules may be the chief cause of their inactivation. In previous studies, the fragmentation of viral RNA was observed in addition to the photocatalytic degradation of S-proteins (Matsuura et al. 2021; Nakano et al. 2022), and OH radicals may be involved in both the oxidative degradations.

We revealed an additive effect of metals (Cu and Ag) with N-TiO_2 on the inactivation of SARS-CoV-2. A comparison of the inactivation activity of N-TiO_2 and Cu/N-TiO_2 (Fig. 7) suggested that inactivation was enhanced by the presence of Cu owing to photoirradiation-induced increased generation of reactive oxygen species. The time-dependent inactivation by Ag + Cu/N-TiO_2 under dark conditions was attributed to Ag (Fig. 7). Furthermore, the most effective inactivation of SARS-CoV-2 was observed when Ag + Cu/N-TiO_2 was exposed to light for 60 min. Taken together, these results suggest that N-TiO_2 triggers light-induced SARS-CoV-2 inactivation and is enhanced by Cu loading and further enhanced by the addition of Ag. The promotion of viral inactivation may result from multiple action mechanisms. Surface-coated copper and silver have been known to exert direct antiviral activity against numerous types of viruses, with or without viral envelopes (Thurman et al. 1989; Rai et al. 2020). Solid-state silver has also been reported to inactivate enveloped influenza A viruses as well as SARS-CoV-2 more strongly than the same amount of copper (Minoshima et al. 2016). This finding supports the results shown in Fig. 4, which revealed a stronger inactivation activity of Ag + Cu/N-TiO_2 compared with Cu/N-TiO_2 in dark conditions. Another possible mechanism of action is that viral particles are adsorbed by Cu or Ag and inactivated at active sites near the photocatalytic surface, such as holes and OH radicals generated by light irradiation in the vicinity, and the difference in the inactivation activities of Cu/N-TiO_2 and Ag + Cu/N-TiO_2 may reflect the difference in affinity of Cu and Ag toward the viral surface.

The SARS-CoV-2 Delta variant was reported to spread more rapidly than the Wuhan strain (Kupferschmidt and Wadman 2021). Furthermore, the Omicron variant was reported to show more effective transmission (Torjesen 2021; Dehury et al. 2021). These variants temporarily became predominant, suggesting that emerging variants may be prevalent in future. In the present study, visible-light irradiation of Ag + Cu/N-TiO_2 inactivated three SARS-CoV-2 strains, including the Wuhan, Delta, and Omicron variants (Fig. 5). Amino acid substitutions in the S-protein, which binds to ACE2 on the human cell membrane of both the Delta and Omicron variants on the surface of virus may alter the structure or charge state of the S-protein and affect its inactivation (Han et al. 2022). Despite some differences in the amino acid sequences of the S-proteins, the inactivation mechanism was partially considered to occur due to some changes of these proteins by hole and OH radicals generated via photocatalytic activity, as was the case with the Wuhan strain. If the adsorption properties against viral particles differ for Ag and Cu, Ag + Cu/N-TiO_2 may be applicable to a wide range of mutations, and thus may inactivate new SARS-CoV-2 variants.

Acknowledgements Toyota Central R&D Labs, Inc. financially supported this research, and Takashi Matsuyama, Shu Saeki, Satoru Kosaka, Yoriko Matsuoka, and Takao Imaeda

were employees of Toyota Central R&D Labs, Inc. for the duration of this study. Yasushi Itoh has no financial relationships to disclose.

Supporting information Figure S1—XRD patterns of three types of photocatalyst. The crystal structure of all synthesized powder is the anatase phase (JCPDS file 21-1272). The crystallite diameters of all synthesized powder are calculated to be about 20 nm from Scherrer's equation.

Figure S2—The optical absorption spectra of three types of photocatalyst and the base TiO_2 powder. The vertical axis was Kubelka-Munk corrected based on the diffuse reflection spectrum data.

Figure S3—Spectrum of a light source using a fluorescent lamp with a UV-cut film.

Author contributions All authors except for YA contributed to the study conception and design. Material preparation and data collection and analysis were performed by TM, SS, SK, YM, YA, YI, and TI. The first draft of the manuscript was written by Takashi Matsuyama and all authors commented on previous versions of the manuscript. All authors read and approved the final manuscript.

Funding Takashi Matsuyama, Shu Saeki, Satoru Kosaka, Yoriko Matsuoka, Yoshifumi Aoki, and Takao Imaeda have received research support from Toyota Central R&D Labs, Inc.

Data availability The datasets were included in electric supplementary materials.

Declarations

Competing interests Yasushi Itoh has no financial relationships to disclose. Takashi Matsuyama, Shu Saeki, Satoru Kosaka, Yoriko Matsuoka, Yoshifumi Aoki, and Takao Imaeda were employees of Toyota Central R&D Labs, Inc. for the duration of this study.

References

Asahi R, Morikawa T, Ohwaki T, Aoki K, Taga Y (2001) Visible-light photocatalysis in nitrogen-dopedtitanium oxides. Science 293:269–271. https://doi.org/10.1126/science.1061051

Asahi R, Morikawa T, Irie H, Ohwaki T (2014) Nitrogen-doped titanium dioxide as visible-light-sensitive photocatalyst: designs, developments, and prospects. Chem Rev 114:9824–9852. https://doi.org/10.1021/cr5000738

Dehury B, Raina V, Misra N, Suar M (2021) Effect of mutation on structure, function and dynamics of receptor binding domain of human SARS-CoV-2 with host cell receptor ACE2: a molecular dynamics simulations study. J Biomol Struct Dyn 39:7231–7245. https://doi.org/10.1080/07391102.2020.1802348

Feng B, Xu K, Gu S, Zheng S, Zou Q, Xu Y, Yu L, Lou F, Yu F, Jin T, Li Y, Sheng J, Yen HL, Zhong Z, Wei J, Chen Y (2021) Multi-route transmission potential of SARS-CoV-2 in healthcare facilities. J Hazard Mater 402:123771. https://doi.org/10.1016/j.jhazmat.2020.123771

Finkelstein E, Rosen GM, Rauckman EJ (1980) Spin trapping. Kinetics of the reaction of superoxide and hydroxyl radicals with nitrones. J Am Chem Soc 102:4994–4999. https://doi.org/10.1021/ja00535a029

Finkelstein E, Rosen GM, Rauckman EJ (1982) Production of hydroxyl radical by decomposition of superoxide spin-trapped adducts. Mol Pharmacol 21:262–265

Han P, Li L, Liu S, Wang Q, Zhang D, Xu Z, Han P, Li X, Peng Q, Su C, Huang B, Li D, Zhang R, Tian M, Fu L, Gao Y, Zhao X, Liu K, Qi J, Gao GF, Wang P (2022) Receptor binding and complex structures of human ACE2 to spike RBD from omicron and delta SARS-CoV-2. Cell 185:630–640. https://doi.org/10.1007/BF00167182

Kakuma Y, Nosaka A, Nosaka Y (2015) Difference in TiO_2 photocatalytic mechanism between rutile and anatase studied by the detection of active oxygen and surface species in water. Phys Chem Chem Phys 17:18691–18698

Kampf G, Grotheer D, Steinmann J (2005) Efficacy of three ethanol-based hand rubs against feline calicivirus, a surrogate virus for Norovirus. J Hosp Infect 60:144–149. https://doi.org/10.1016/j.jhin.2004.12.005

Katoh R, Furube A, Yamanaka K, Morikawa T (2010) Charge separation and trapping in N-doped TiO_2 photocatalysts: a time-resolved microwave conductivity study. J Phys Chem Lett 1:3261–3265. https://doi.org/10.1021/jz1011548

Killingley B, Mann AJ, Kalinova M, Boyers A, Goonawardane N, Zhou J, Lindsell K, Hare SS, Brown J, Frise R, Smith E, Hopkins C, Noulin N, Löndt B, Wilkinson T, Harden S, McShane H, Baillet M, Gilbert A, Jacobs M, Charman C, Mande P, Nguyen-Van-Tam JS, Semple MG, Read RC, Ferguson NM, Openshaw PJ, Rapeport G, Barclay WS, Catchpole AP, Chiu C (2022) Safety, tolerability and viral kinetics during SARS-CoV-2 human challenge in young adults. Nat Med 28:1031–1041. https://doi.org/10.1038/s41591-022-01780-9

Koppenol WH, Liebman JF (1984) The oxidizing nature of the hydroxyl radical. A comparison with the Ferry1 Ion (FeO^{2+}). J Phys Chem 88:99–101

Kupferschmidt K, Wadman M (2021) Delta variant triggers new phase in the pandemic. Science 372:1375–1376. https://doi.org/10.1126/science.372.6549.1375

Makino K, Mossoba MM, Riesz P (1982) Chemical effects of ultrasound on aqueous solutions. Evidence for hydroxyl and hydrogen free radicals (OH and H) by spin trapping. J Am Chem Soc 104:3537–3539. https://doi.org/10.1021/ja00376a064

Matsuura R, Lo CW, Wada S, Somei J, Ochiai H, Murakami T, Saito N, Ogawa T, Shinjo A, Benno Y, Nakagawa M, Takei M, Aida Y (2021) SARS-CoV-2 disinfection of air and surface contamination by TiO_2 photocatalyst-mediated damage to viral morphology, RNA, and protein. Viruses 13:942. https://doi.org/10.3390/v13050942

Minoshima M, Lu Y, Kimura T, Nakano R, Ishiguro H, Kubota Y, Hashimoto K, Sunada K (2016) Comparison of the antiviral effect of solid-state copper and silver compounds. J Hazard Mater 312:1–7. https://doi.org/10.1016/j.jhazmat.2016.03.023

Morikawa T, Irokawa Y, Ohwaki T (2006) Enhanced photocatalytic activity of TiO_2−xNx loaded with copper ions under visible-light irradiation. Appl Cat A: General 314:123–127. https://doi.org/10.1016/j.apcata.2006.08.011

Nakamura S, Ando N, Sato M, Ishihara M (2020) Ultraviolet irradiation enhances the microbicidal activity of silver nanoparticles by hydroxyl radicals. Int J Mol Sci 21:3204–3215

Nakano R, Yamaguchi A, Sunada K, Nagai T, Nakano A, Suzuki Y, Yano H, Ishiguro H, Miyauchi M (2022) Inactivation of various variant types of SARS-CoV-2 by indoor-light-sensitive TiO_2-based photocatalyst. Sci Rep 12:5804. https://doi.org/10.1038/s41598-022-09402-7

Ohwaki T, Saeki S, Aoki K, Morikawa T (2016) Evaluation of photocatalytic activities and characteristics of Cu- or Fe-modified nitrogen-doped titanium dioxides for applications in environmental purification. Jpn J Appl Phys 55:01AA05

Pilaquinga F, Morey J, Torres M, Seqqat R, Piña MLN (2021) Silver nanoparticles as a potential treatment against SARS-CoV-2: a review. Wiley Interdiscip Rev Nanomed Nanobiotechnol 13:e1707. https://doi.org/10.1002/wnan.1707

Prakash J, Cho J, Mishra YK (2022) Photocatalytic TiO_2 nanomaterials as potential antimicrobial and antiviral agents: scope against blocking the SARS-COV-2 spread. Micro Nano Eng 14:100100

Prather KA, Wang CC, Schooley RT (2020) Reducing transmission of SARS-CoV-2. Science 368:1422–1424. https://doi.org/10.1126/science.abc6197

Rai PK, Usmani Z, Thakur VK, Gupta VK, Mishra YK (2020) Tackling COVID-19 pandemic through nanocoatings: confront and exactitude. Curr Res Green Sustain Chem 3:100011

Sunada K, Minoshima M, Hashimoto K (2012) Highly efficient antiviral and antibacterial activities of solid-state cuprous compounds. J Hazard Mater 235–236:265–270. https://doi.org/10.1016/j.jhazmat.2012.07.052

Thurman R, Bitton GCP (1989) The molecular mechanisms of copper and silver ion disinfection of bacteria and viruses. CRC Crit Rev Environ Control 18:295–315. https://doi.org/10.1080/10643388909388351

Torjesen I (2021) Covid-19: Omicron may be more transmissible than other variants and partly resistant to existing vaccines, scientists fear. BMJ 375:n2943. https://doi.org/10.1136/bmj.n2943

Uema M, Yonemitsu K, Momose Y, Ishii Y, Tateda K, Inoue T, Asakura H (2021) Effect of the photocatalyst under visible-light irradiation in SARS-CoV-2 stability on an abiotic surface. Biocontrol Sci 26:119–125. https://doi.org/10.4265/bio.26.119

van Doremalen N, Bushmaker T, Morris DH, Holbrook MG, Gamble A, Williamson BN, Tamin A, Harcourt JL, Thornburg NJ, Gerber SI, Lloyd-Smith JO, de Wit E, Munster VJ (2020) Aerosol and surface stability of SARS-CoV-2 as compared with SARS-CoV-1. N Engl J Med 382:1564–1567. https://doi.org/10.1056/NEJMc2004973

Zhang J, Nosaka Y (2015) Photocatalytic oxidation mechanism of methanol and the other reactants in irradiated TiO_2 aqueous suspension investigated by OH radical detection. Appl Catal B: Environ 166–167:32–36

Zhou P, Yang XL, Wang XG, Hu B, Zhang L, Zhang W, Si HR, Zhu Y, Li B, Huang CL, Chen HD, Chen J, Luo Y, Guo H, Jiang RD, Liu MQ, Chen Y, Shen XR, Wang X, Zheng XS, Zhao K, Chen QJ, Deng F, Liu LL, Yan B, Zhan FX, Wang YY, Xiao GF, Shi ZL (2020) A pneumonia outbreak associated with a new coronavirus of probable bat origin. Nature 579:270–273. https://doi.org/10.1038/s41586-020-2012-7

Zhu N, Zhang D, Wang W, Li X, Yang B, Song J, Zhao X, Huang B, Shi W, Lu R, Niu P, Zhan F, Ma X, Wang D, Xu W, Wu G, Gao GF, Tan W, China Novel Coronavirus Investigating and Research Team (2020) A novel coronavirus from patients with pneumonia in China, 2019. N Engl J Med 382:727–733. https://doi.org/10.1056/NEJMoa2001017